

Appearance-Based Gaze Estimation via Gaze Decomposition and Single Gaze Point Calibration

Zhaokang Chen Bertram E. Shi
 The Hong Kong University of Science and Technology
 Hong Kong SAR

zchenbc@connect.ust.hk, eebert@ust.hk

Abstract

Appearance-based gaze estimation provides relatively unconstrained gaze tracking. However, subject-independent models achieve limited accuracy partly due to individual variations. To improve estimation, we propose a novel gaze decomposition method and a single gaze point calibration method, motivated by our finding that the inter-subject squared bias exceeds the intra-subject variance for a subject-independent estimator. We decompose the gaze angle into a subject-dependent bias term and a subject-independent difference term between the gaze angle and the bias. The difference term is estimated by a deep convolutional network. For calibration-free tracking, we set the subject-dependent bias term to zero. For single gaze point calibration, we estimate the bias from a few images taken as the subject gazes at a point. Experiments on three datasets indicate that as a calibration-free estimator, the proposed method outperforms the state-of-the-art methods that use single model by up to 10.0%. The proposed calibration method is robust and reduces estimation error significantly (up to 35.6%), achieving state-of-the-art performance for appearance-based eye trackers with calibration.

1. Introduction

As an important cue about people’s intent, eye gaze has been used in many promising real-world applications, such as human-computer interfaces [4, 22, 27], human-robot interaction [15], virtual reality [23, 26], social behavioral analysis [14] and health care [12]. These successes have led to gaze tracking attracting more and more attention.

To date, most eye trackers have relied upon active illumination, e.g. infrared illumination used in pupil center corneal reflections (PCCR). While these provide high accuracy, they also place strong constraints on users’ head movements. Accuracy rapidly degrades as the head pose changes. Nonetheless, these techniques are commonly used

in laboratory settings where high accuracy is required. Researchers have proposed many novel methods to alleviate constraints on head movement, which will enable more real-world applications that require unconstrained gaze estimation in more flexible environments, e.g. [2, 6, 9, 10, 11, 18, 25, 33, 34, 35, 37, 41]. However, a common disadvantage of active illumination approaches is that they are also relatively costly, as they rely upon custom hardware to provide the required illumination.

Appearance-based gaze estimation estimates the gaze target (2D position on a given plane or 3D gaze angles) based on RGB images. It is attracting more and more attention because it provides relatively unconstrained gaze tracking and requires only commonly available off-the-shelf cameras. However, obtaining high accuracy is very challenging due to large variability caused by factors such as differences in individual appearance, head pose, and illumination [43]. The application of deep convolutional neural networks (CNNs) to this problem has reduced estimation error significantly [41]. There are a large number of high quality real and synthetic datasets covering a wide range of these variations [9, 11, 18, 30, 32, 33, 36, 37, 41]. Using these datasets, it has been shown that deep CNNs can learn to compensate for the variability [3, 5, 7, 18, 19, 28, 42].

Unfortunately, the estimation error of subject-independent appearance-based methods is still higher than that achievable using active illumination, e.g. $\sim 5^\circ$ vs $\sim 1^\circ$. Thus, further work must be done to reduce this error.

One way to further reduce estimation error is through personal calibration. PCCR-based eye trackers typically require an initial multiple gaze point calibration step before they are used. The user must gaze at a number (typically nine points on a three by three grid) of gaze targets sequentially [13]. This enables subject-specific parameters of a geometric 3D eye model to be estimated. A similar calibration procedure has been proposed for appearance-based methods, where some parameters of the estimator are fine-tuned based on the calibration data [18, 20, 21]. However, multiple gaze point calibration is time-consuming and may

not be applicable in some situations, e.g. in screen-free applications, it is difficult to provide multiple targets for calibration.

In this article, we propose a gaze decomposition method for appearance-based gaze estimation, and a single gaze point calibration method that requires the user to gaze only at a single point. This is more widely applicable than multiple gaze point calibration e.g. for screen-free applications, since the camera, which should always be visible, can be used as the calibration point. Our experimental results demonstrate that the gaze decomposition significantly improves estimation performance. Using only single gaze point calibration results in state-of-the-art performance for appearance-based eye trackers with calibration. Further reduction in estimation error can be obtained by using multiple gaze points.

These two methods are based on the assumption that there exists person-dependent bias that can not be estimated from the images. It is known that there is a deviation between the visual axis and the optic axis of an eye, and that this deviation varies from person to person [1, 13]. Our own experimental results confirm this finding. For a subject-independent estimator, the estimation bias varies significantly across subjects but seems to be relatively constant across different gaze angles for the same subject (see Fig. 1). Thus, we decompose the gaze estimate into a subject-dependent bias term and a subject-independent gaze difference term between true gaze and the bias. The difference term is estimated by a deep convolutional neural network. For calibration-free tracking, we set the subject-dependent bias term to zero. For single gaze point calibration, we estimate the bias term from images taken as the subject gazes at a single gaze point.

We evaluate the performance of calibration-free subject-independent gaze estimation and the single gaze point calibration thoroughly. We evaluate through within- and cross-dataset settings on three public datasets: the MPIIGaze [41], the EYEDIAP [11] and the Columbia [32] datasets. Our experimental results demonstrate that as a calibration-free estimator, our proposed method outperforms the state-of-the-art methods that use single model on the MPIIGaze and the EYEDIAP datasets with a gain up to 10.0%. Calibrating on only a few images (about 9) can significantly reduce the estimation error, achieving a gain up to 35.6% in comparison to the calibration-free estimator, and that the calibration is robust to the location of calibration points.

2. Related work

2.1. Appearance-based gaze estimation

Methods for appearance-based gaze estimation directly regress from images to gaze estimate. In principal, given enough training data, they may be able to address the large

variability in real-world situation, achieving relatively unconstrained gaze tracking.

Past approaches to this problem have included k-Nearest Neighbors [33, 29], Support Vector Regression [29] and Random Forests [33]. More recently, the application of deep CNNs to this problem has received increasing attention. Zhang *et al.* proposed the first deep CNN for gaze estimation in the wild [41, 43], which they showed improved accuracy significantly. To further improve the accuracy, others have proposed enhancements, such as employing the information outside the eye region [18, 42], focusing on the head-eye relationship [7, 28] and extracting better information from the eye images [3, 5, 19, 24, 39].

Krafka *et al.* proposed a CNN with multi-region input (an image of the face, images of both eyes and a face grid) to estimate the gaze target on screens of mobile devices [18]. Zhang *et al.* proposed a network that takes the full face image as input and adopts a spatial weights method to emphasize features from particular face regions [42]. This work has shown that regions of the face other than the eyes also contain information about the gaze angle.

Some work has concentrated on the head-eye relationships. Deng and Zhu estimated the head pose in camera-centric coordinates, the gaze angles in head-centric coordinates, and then combined them geometrically [7]. Ranjan *et al.* applied a branching architecture, where parameters are switched according to a clustering of head pose angles into different groups [28].

Other work has focused on extracting better information from eye images. Cheng *et al.* studied the “two eye asymmetry problem”: the estimation accuracy are different for both eyes. They proposed a novel network that relied on the high quality eye images for training [5]. Yu *et al.* proposed to estimate the eye landmark locations and gaze directions jointly [39]. Park *et al.* proposed to learn an intermediate pictorial representation of the eyes for better gaze estimation [24]. Chen and Shi proposed to use dilated-convolutions to extract features at high resolution, as large changes in gaze angle may result in only small changes in eye appearance [3]. Lian *et al.* improved accuracy by using images from multiple cameras [19].

2.2. Personal calibration

Calibration for appearance-based methods has received little attention to date. To our knowledge, the first implementation of personal calibration was in iTracker [18]. After training a subject independent network, they calibrated by training a person-dependent Support Vector Regressor on the features from the last fully-connected layer using images collected as the subject gazed at 13 different locations. Error was reduced by about 20% when calibrated on the full set of 13 points, but increased when only calibrated on a subset of 4 points, most likely due to overfitting.

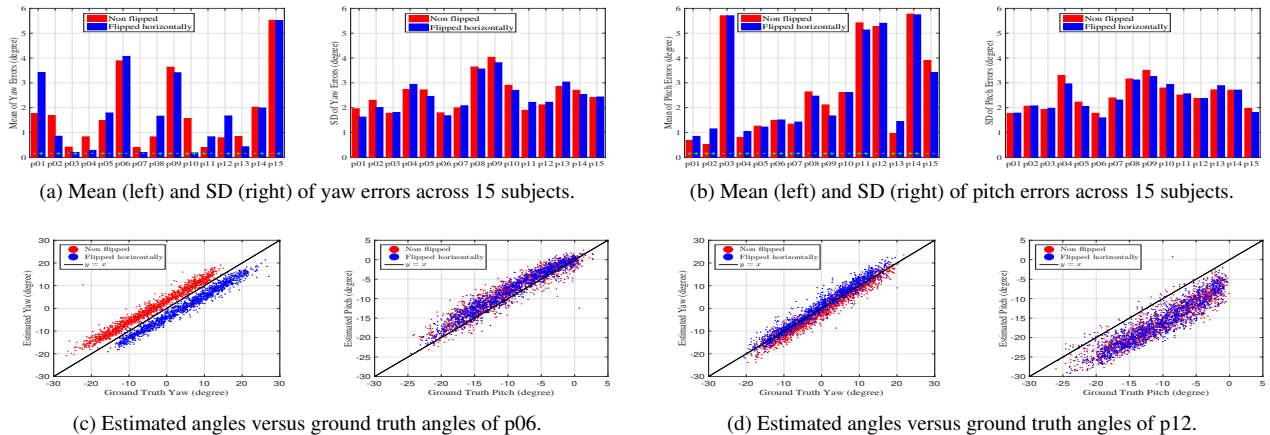


Figure 1. Error analysis of a subject-independent estimator on the MPIIGaze dataset. Mean and standard deviation of the yaw (a) and pitch (b) angles for each subject. The green + or - indicate the sign of the mean. Scatter plots of the estimated angles versus the ground truth of two subjects, p06 (c) and p12 (d). Half of the images are non-flipped (red) and half are flipped horizontally (blue). There exists person-dependent bias that vary across subjects, but is quite constant across gaze angles. Better viewed in color and zoomed in.

Lindén *et al.* proposed a network that includes some person-dependent latent parameters [20]. During training, these parameters are learned from the training data. During testing, these parameters can be estimated by minimizing the estimation error in the calibration set with the rest of the network fixed. The calibration set required ranged from 45-100 images and was collected as the subject gazed at multiple points. Liu *et al.* proposed a differential approach for calibration [21]. They trained a subject-independent Siamese network to estimate the gaze angle difference between two images of the same subject. During testing, they used this network to estimate gaze differences between the input image and nine calibration images taken as the subject gazed at different locations, and averaged the resulting estimates.

In comparison to the work described above, our proposed method achieves better accuracy, while requiring a smaller number of images taken as the subject gazes at only a single point.

3. Methodology

3.1. Analysis of estimation error

Fig. 1 analyzes estimation error on the MPIIGaze [41] dataset made by a state-of-the-art subject-independent gaze estimator [3]. Fig. 1(a) and (b) show the mean and standard deviation (SD) of the yaw and pitch error for different subjects and for both original and horizontally flipped images. These results show that the errors in both yaw and pitch angles are generally biased. The bias vary across subjects, whereas the SDs are relatively stable. When the images are flipped horizontally, the yaw bias typically has similar magnitude, but different sign, while the pitch bias remains similar. The mean squared bias across subjects (16.2 deg^2) exceeds the mean intra-subject variance (12.9 deg^2), indi-

cating that the bias is a significant contributor to the error.

Fig. 1(c) and (d) compare the estimated angles and the ground truth of two subjects. The scatter plots indicate that the bias is quite constant across gaze angles, but varies between subjects. As the data of each subject exhibits considerable variability in illumination, we hypothesize that a major determinant of this bias is due to user differences.

3.2. Gaze decomposition

Motivated by the previous findings, we assume that there exists person-dependent bias that can not be estimated from the images. This assumption is supported by the fact that there exists a person-dependent deviation between the visual axis (the line connecting the nodal point with the fovea) and the optic axis (the line connecting the nodal point with the pupil center), but is not observable from the appearance of the eye [1, 13]. This assumption can be formally formulated as follows, where we use i to denote the index of subject and j the index of image:

$$X_{i,j} = \mathcal{F}(c_i, t_{i,j}), \quad (1)$$

$$g_{i,j} = t_{i,j} + b_i, \quad (2)$$

where $X_{i,j}$ an image of subject i with image index j , \mathcal{F} an arbitrary function, c_i the appearance feature of subject i , $t_{i,j}$ the gaze difference, $g_{i,j}$ the true gaze expressed as yaw and pitch, and b_i the person-dependent bias. One can not estimate b_i from $X_{i,j}$.

Under this assumption, we decompose gaze estimates, \hat{g} , into the sum of a subject-dependent bias term, \hat{b} , and a subject-independent difference term, \hat{t} :

$$\hat{g}(X_{i,j}) = \hat{t}(X_{i,j}) + \hat{b}_i. \quad (3)$$

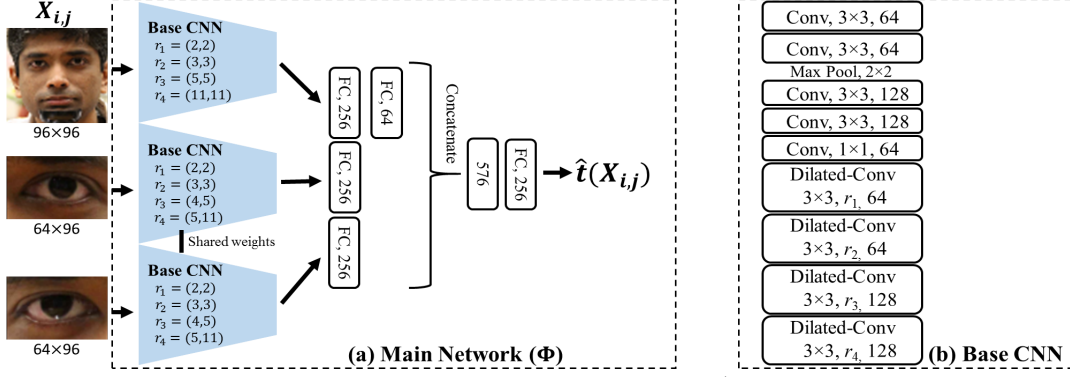


Figure 2. Architecture of the proposed network. (a) The main network that outputs $\hat{t}(X_{i,j})$ based on the input image $X_{i,j}$. (b) The base CNN is the basic component of (a). FC denotes fully-connected layers, Conv denotes convolutional layers, Dilated-Conv denotes dilated-convolutional layers, and r is the dilation rate of the dilated-convolutional layer.

Note that a model which directly estimates the gaze angles is equivalent to a model with $\hat{b}_i \equiv 0, \forall i$. We describe below how to estimate \hat{b}_i under different scenarios: training, calibration-free estimation and calibration.

3.3. The proposed network

The architecture of our proposed network is presented in Fig. 2. The general architecture is inspired by iTracker [18] and Dilated-Net [3]. It takes an image of the face and images of both eyes as input. The output of the network $\hat{t}(X_{i,j})$ is used to generate gaze estimates according to (3).

The input images $X_{i,j}$ are first fed to three base CNNs. The architecture of the base CNN is shown in Fig. 2(b). It has five convolutional layers, one max-pooling layer and four dilated-convolutional layers [38] with different dilation rate, r . The strides for all (dilated-) convolutional layers are 1. The weights of the first four convolutional layers are transferred from VGG-16 [31] pre-trained on the ImageNet dataset [8]. The two base CNNs that take the eyes as input share the same weights. The feature maps extracted by the base CNNs are then fed to fully-connected (FC) layers, concatenated, fed to another FC layer followed by a linear output layer to output $\hat{t}(X_{i,j})$. We denote the parameters of this network as Φ .

Rectified Linear Units (ReLUs) are used as the activation function. Zero-padding is applied to regular convolutional layers and no padding is applied to dilated-convolutional layers. Batch renormalization layers [16] are applied to all layers trained from scratch. Dropout layers with dropout rates of 0.5 are applied to all FC layers.

Training. Based on (1)(2)(3), we train the network by solving the following optimization problem:

$$\min_{\Phi, \beta} \left(\sum_{i,j} (g_{i,j} - \hat{t}(X_{i,j}; \Phi) - \beta_i)^2 + \lambda \left| \sum_i \beta_i \right| \right) \quad (4)$$

where β_i are estimates of the bias for subjects in the training set which are learned. The second term is a regularizer that ensures average subject-dependent bias over the training set is zero. Since this mean bias is arbitrary, the training is insensitive to the value of λ . The β_i could also be estimated by calculating the individual mean over the training set, but this would be time consuming, given the large size of training set, especially since we use online data augmentation.

We use Adam optimizer with default parameters in TensorFlow and a batch size of 64. An initial learning rate of 0.001 is used. It is divided by 10 after every ten epochs. The training proceeds for 35 epochs. We apply online data augmentation including random cropping, scaling, rotation and horizontal flipping. As the bias changes if the images are flipped horizontally, we considered the non-flipped and flipped images as belonging to different subjects.

Testing and calibration. During testing, gaze estimates are generated according to (3). For a new subject m , if no calibration images are available, we set $\hat{b}_m = 0$.

Given a calibration set \mathcal{D}_c , which includes image-gaze pairs for a subject m , $\{(X_{m,j}, g_{m,j}), j = 1, 2, \dots, |\mathcal{D}_c|\}$, we set $\hat{b}_m = \tilde{b}_m$, where

$$\tilde{b}_m = \frac{1}{|\mathcal{D}_c|} \sum_{X_{m,j} \in \mathcal{D}_c} (g_{m,j} - \hat{t}(X_{m,j})), \quad (5)$$

where $|\cdot|$ represents cardinality. After calibration according to (5), the mean squared error (MSE) of our gaze estimate (3) over the test set can be expressed as follows:

$$\begin{aligned} \text{MSE} &= \text{Tr} \left\{ \mathbb{E}_k [g_{m,k} - \hat{t}(X_{m,k}) - \tilde{b}_m] \right. \\ &\quad \left. [g_{m,k} - \hat{t}(X_{m,k}) - \tilde{b}_m]^\top \right\} \\ &= \text{Tr} \left\{ \Sigma_{\hat{t}_m} \right\} + \text{Tr} \left\{ (\mu_m - \tilde{b}_m)(\mu_m - \tilde{b}_m)^\top \right\} \\ &\geq \text{Tr} \left\{ \Sigma_{\hat{t}_m} \right\}, \end{aligned} \quad (6)$$

where $\Sigma_{\hat{t}_m} \triangleq \text{Cov}_k[g_{m,k} - \hat{t}(X_{m,k})]$ and $\mu_m \triangleq \mathbb{E}_k[g_{m,k} - \hat{t}(X_{m,k})]$. The equality holds when $\tilde{b}_m = \mu_m$. We expect there to be a good match between μ_m and \tilde{b}_m if \mathcal{D}_c contains a large range of gaze directions and a large number of samples (i.e., multiple gaze points calibration). For single gaze point calibration, where \mathcal{D}_c only covers a small range of gaze angles, there may be a systematic gaze position dependent offset between the two. This illustrates the challenge of single gaze point calibration. Although our results use angular error between two 3D vectors but not the MSE, similar considerations apply.

Preprocessing. We apply the modified data normalization method introduced in [40]. This method rotates and scales an image so that the resulting image is taken by a virtual camera facing towards a reference point on the face at a fixed distance and canceling out the roll angle of the head. The images are normalized by perspective warping, converted to gray scale and histogram-equalized. The ground truth gaze angles are also normalized correspondingly by rotation but not scaling. For automatically detected landmarks we use dilb [17].

4. Experiments

We evaluated our proposed network through cross-subject evaluation in both within- and cross-dataset settings. We evaluated the calibration-free estimation error and the performance gain from single gaze point calibration.

4.1. Within-dataset evaluation

Datasets. We used the MPIIGaze [41] and the EYEDIAP [11] datasets. The MPIIGaze dataset contains full face images of 15 subjects (six female, five with glasses). It provides an ‘‘Evaluation Subset’’, which contains 3,000 randomly selected images for each subject. Within this subset, half of the images are flipped horizontally. We conducted 15-fold leave-one-subject-out cross-validation to train and test on this evaluation subset. The reference point for image normalization was set to the center of the face.

The EYEDIAP dataset contains full face videos with three gaze targets (continuous screen target, discrete screen target and floating target) and two types of head pose (static and dynamic). We used the data from screen targets, which involve 14 subjects (three female, none with glasses). For calibration-free estimation, we followed the experiment described in [42], i.e., five-fold cross-validation on four VGA videos (both screen targets with both types of head pose) sampled at 2 fps (about 1,200 images per subject). For calibration evaluation, we conducted leave-one-subject-out cross-validation on two VGA videos (continuous screen target with both types of head pose) sampled at 15 fps (about 3,500 images per subject). We chose continuous screen tar-

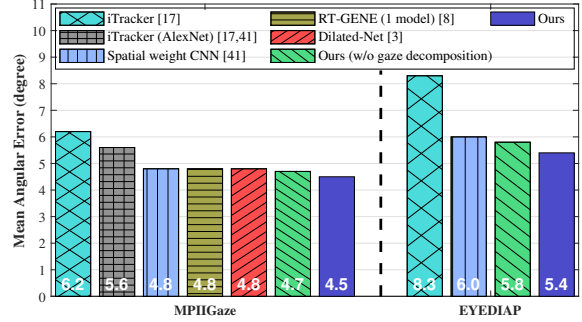


Figure 3. Mean angular error of calibration-free estimation on the MPIIGaze and the EYEDIAP dataset.

get because they had sufficient annotation to remove outliers, e.g. images during blinking. We use higher sampling rate to obtain more samples. The reference point for image normalization was set to the midpoint of both eyes.

Results of calibration-free estimation. We compared with several baselines that used single model: iTracker [18, 42], spatial weights CNN [42], RT-GENE [9] and Dilated-Net [3]. All of these methods used face images (or face plus eye images) as input. We also trained a network without gaze decomposition for ablation study.

The results are shown in Fig. 3. On the MPIIGaze dataset, our proposed network achieved 4.5° mean angular error, which outperformed the state-of-the-art 4.8° [3, 9, 42] by 6.3%. On the EYEDIAP dataset, it achieved 5.4°, which outperformed the state-of-the-art 6.0° [42] by 10.0%. The gain may partly due to the use of the modified data normalization method [40] and our proposed gaze decomposition. Note that RT-GENE achieved 4.3° on the MPIIGaze dataset by ensembling four models, however, our network did not achieve significant improvement by ensembling.

Calibration. We used a strategy to mimic single gaze point calibration (SGPC). To obtain the calibration set \mathcal{D}_c for a calibration point in the 2D (yaw, pitch) gaze space, we randomly selected $|\mathcal{D}_c|$ images from the test set whose true gaze angles differed from the calibration point by less than 2°. We calibrated on \mathcal{D}_c according to (5), where we set the true gaze angle to the mean of the gaze angles in the calibration set. We tested on the images not belonging to \mathcal{D}_c . We discarded a calibration point if less than $|\mathcal{D}_c|$ images met the 2° requirement. Note that one gaze point can have multiple calibration samples.

For multiple gaze point calibration (MGPC), we randomly selected $|\mathcal{D}_c|$ images from the test set with different gaze directions as \mathcal{D}_c , calibrated according to (5) and tested on the images not belonging to \mathcal{D}_c .

We also calculated a lower bound on the calibration per-

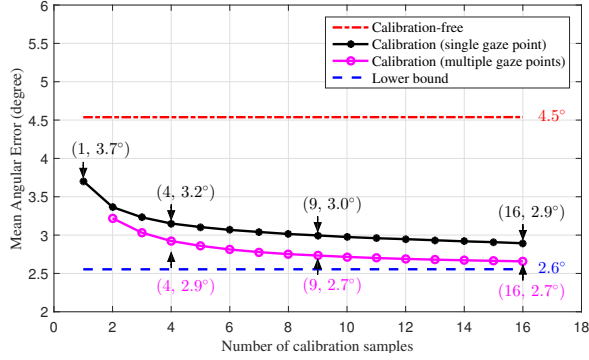


Figure 4. Mean angular error in camera coordinates as a function of number of calibration samples on the MPIIGaze dataset.

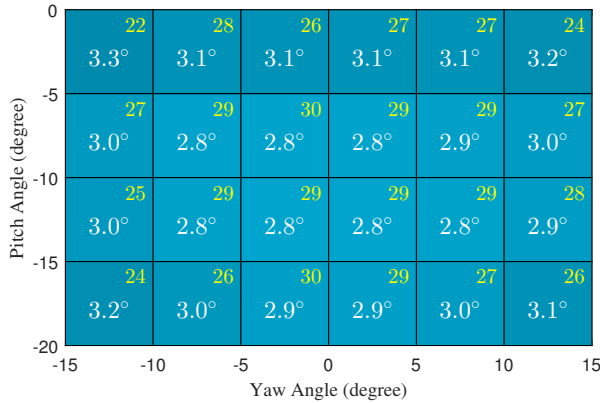


Figure 5. Mean angular error (white) in camera coordinates and the number of subjects that benefit among 30 subjects (yellow) when calibrated at different locations on the MPIIGaze dataset. Each $5^\circ \times 5^\circ$ region includes a 10×10 grid of calibration points. $\bar{E} = 4.5^\circ$, $\underline{E} = 2.6^\circ$, $|\mathcal{D}_c| = 9$.

formance by estimating the bias from all images in the test set and evaluating on the test set.

We denote the mean angular error of the calibration-free subject-independent tracking as \bar{E} and the error of the calibration lower bound as \underline{E} .

Results of calibration. In the MPIIGaze dataset, since half of the images were flipped and we considered the data from the non-flipped and flipped images separately when computing the bias and the accuracy, each subject generates two accuracies (30 in total). Note that none of the flipped/non-flipped images of the test subject were included in the training set. To evaluate the overall performance of SGPC across different calibration points and subjects, we randomly selected a calibration point for each subject according to a uniform distribution. We then calculated the calibration performance according to the calibration procedure described above. We repeated this procedure for 5,000 times. For MGPC, we randomly sampled $|\mathcal{D}_c|$ images for calibration

Method	Error	Remarks
Liu <i>et al.</i> [21]*	4.7°	Calibrated on 9 samples
Lindén <i>et al.</i> [20]	2.9°	Calibrated on > 100 samples
Person-specific CNN [43]*	5.4°	Subject-independent
	2.5°	Trained on 2,500 and tested on 500 samples
Ours	3.9°	Calibration-free
Single gaze point calibration (ours)	3.2°	Calibrated on 1 sample
	2.7°	Calibrated on 4 samples
	2.6°	Calibrated on 9 samples
	2.5°	Calibrated on 16 samples
Multiple gaze point calibration (ours)	2.5°	Calibrated on 4 points
	2.4°	Calibrated on 9 points
	2.3°	Calibrated on 16 points
Lower bound (ours)	2.2°	Calibrated on 1,500 samples

*These networks used the images of one eye as input, while the others used the images of full face.

Table 1. Results on MPIIGaze in Normalized Space.

as described above and repeated for 5,000 times. We also varied $|\mathcal{D}_c|$ to evaluate its effect.

Fig. 4 presents the mean angular error across different calibration points and subjects. For both calibration methods, as the number of calibration samples increases, the mean error decreases. We only show the results calibrated on no more than 16 samples because the dataset does not have enough samples. SGPC reduced the estimation error significantly. For example, when calibrated on 16 samples, it reduced the error by 1.6° (35.6%) in comparison to calibration-free estimation. MGPC led to further reductions. On average, the gap between SGPC to MGPC was about 0.2° (4.4% of the error of the calibration-free estimator). This gap suggests that the bias is not constant across different gaze angles.

We evaluated the calibration performance when calibrated at different locations by creating a grid of calibration points which were uniformly distributed in the 2D (yaw, pitch) gaze space with a step of 0.5° in each axis. We set $|\mathcal{D}_c| = 9$, since the error reduction from our above experiment begins to saturate at this point. Fig. 5 presents the mean angular error for calibration points located in different $5^\circ \times 5^\circ$ regions. We only show the results of this region because there are not enough data outside this region. The mean error varies across locations. The error achieved by calibrating at the center of the gaze range is lower than the error achieved by calibrating at the boundary. However, the standard deviation is only 0.15° , indicating that SGPC is quite robust to the location of calibration points. At least 22

out of 30 subjects (73.3%) benefited from it.

In order to compare with the calibration results reported in [20, 21], we converted our results into the normalized space used in their work. We also compared with the person-specific CNN [43], which was trained on 2,500 samples and tested on the remaining 500. The results are presented in Table 1. [21] performed the worst even after calibration, mainly due to that they only use images of one eye as input. When compared with [20], our proposed network achieved lower error if calibrated on more than four samples. When compared with the person-specific CNN, our network achieved the same 2.5° error if calibrated on 16 samples. However, our network required much fewer samples (16 vs 2,500) and over a much smaller range of gaze angles (less than 2°). If we allow calibration over a wider range of gaze angles, we achieved better performance.

For the EYEDIAP dataset, the results are shown in Fig. 6 and Fig. 7. The findings are generally consistent to the ones of the MPIIGaze dataset. The overall performance is worse than that on the MPIIGaze dataset, most likely due to the lower resolution and higher variability of head pose. In Fig. 6, SGPC reduced the estimation error significantly. For example, a 1.2° (25.5%) improvement was achieved when calibrated on 25 samples. On average, the gap between SGPC and MGPC was about 0.5° (10.6% of the error of the calibration-free estimator). In Fig. 7, 0.5° (10.6%) to 1.4° (29.8%) improvement was achieved across different locations. At least 10 out of 14 subjects (71.4%) benefited. Calibrating at the center region also achieved the lowest error. The SD across locations was 0.26° .

As a calibration-free estimator, the mean error achieved in this experiment (4.7°) was better than that in the previous experiment (5.4° , Fig. 3), most likely due to that there were much more training samples in this experiment as it ran at 15 fps instead of 2 fps, and that outliers were removed in this experiment given the extra annotation on this subset.

4.2. Cross-dataset evaluation

Datasets. We trained on the MPIIGaze dataset and tested on the Columbia dataset [32], which has 5,800 full face images of 56 subjects (24 female, 21 with glasses). For each subject, images were collected for each combination of five horizontal head poses ($0^\circ, \pm 15^\circ, \pm 30^\circ$), seven horizontal gaze directions ($0^\circ, \pm 5^\circ, \pm 10^\circ, \pm 15^\circ$) and three vertical gaze directions ($0^\circ, \pm 10^\circ$). We excluded the images corresponding to 10° vertical gaze directions for testing as the MPIIGaze dataset mainly covers pitch angles from -20° to 0° . For SGPC, we used the five images gazing at the same target. These five images have different head pose.

Results. The mean angular error for the calibration-free estimator was $\bar{E} = 5.5^\circ$. The calibration lower bound was $\underline{E} = 4.1^\circ$, indicating the difficulty of cross-dataset evalu-

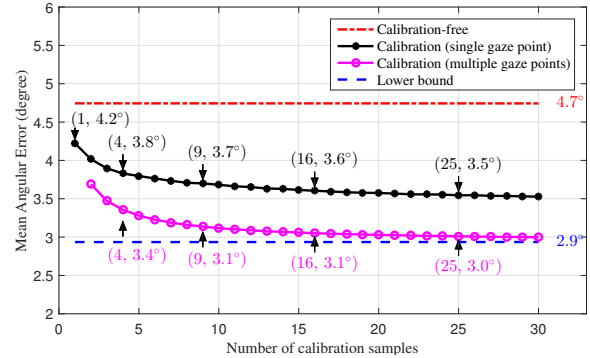


Figure 6. Mean angular error after calibration as a function of number of calibration samples on the EYEDIAP dataset.

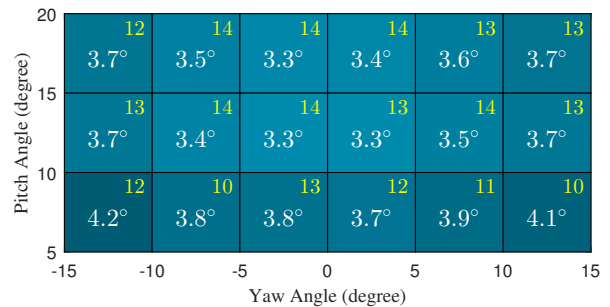


Figure 7. Mean angular error (white) and the number of subjects that benefited among 14 subjects (yellow) when calibrated at different locations on the EYEDIAP dataset. $\bar{E} = 4.7^\circ$, $\underline{E} = 2.9^\circ$, $|\mathcal{D}_c| = 9$.

ation. Fig. 8 shows the calibration performance for different calibration gaze targets. Consistent with our previous results, the performance was poor when calibrated at the four gaze targets at the boundary, i.e., samples with horizontal directions $\pm 15^\circ$. However, for the middle ten calibration points, SGPC reduced the error by 0.8° (14.5%) to 1.1° (20.0%) in comparison to the calibration-free estimator. Between 46 to 51 out of 56 subjects (82.1% to 91.1%) benefited, depending upon the calibration points.

4.3. Ablation study of gaze decomposition

We trained a network without gaze decomposition by setting $\beta_i \equiv 0, \forall i$ in (4) during training. We refer to it as **ND** and the proposed network with gaze decomposition as **D**. In Fig. 3, D network outperformed ND network in calibration-free estimation on the MPIIGaze and EYEDIAP datasets.

We evaluated both networks on the MPIIGaze dataset by the same leave-one-subject-out cross-validation. Fig. 9 presents the results across calibration points and subjects. The D network achieved lower errors in all metric, i.e., calibration-free, SGPC and calibration lower bound. For SGPC, on average, D network achieved a gain about 0.35° from the ND network. The D network achieved smaller cal-

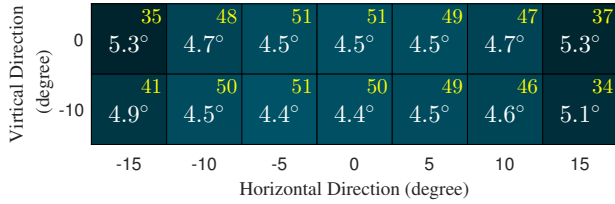


Figure 8. Mean angular error (white) and the number of subjects that benefit among 56 subjects (yellow) when calibrated at different gaze targets. Trained on the MPIIGaze and test on the Columbia dataset. $\bar{E} = 5.5^\circ$, $\underline{E} = 4.1^\circ$, $|\mathcal{D}_c| = 5$.

ibration lower bound (0.3°), indicating that the intra-subject variance was reduced by gaze decomposition. These results are consistent to our model (1)(2): as the person-dependent bias can not be estimated from the images, removing the bias during training according to (4) makes \hat{t} generalizes better.

We also repeated the cross-dataset evaluation for the ND network. The results are shown in Fig. 10, where $\bar{E} = 5.5^\circ$ and $\underline{E} = 4.5^\circ$. Comparing with the results of the D network in Fig. 8, both networks achieved the same 5.5° in calibration-free tracking. However, on average, a gain about 0.4° was achieved by gaze decomposition when both networks were calibrated on five samples.

4.4. Consistency of the learned bias

We evaluated whether the learned biases, i.e., β_i in (4) were consistent for the same subject using leave-one-subject-out (15 fold) cross-validation on the MPIIGaze dataset. For each subject, we computed the mean and SD of the bias across the 14 folds where the subject was included in the training set. Across subjects, the yaw means ranged from -5.4° to 5.4° (SDs from 0.1° to 0.3°). The pitch means ranged from -2.9° to 3.9° (SDs from 0.1° to 0.3°). The mean and SD for each subject is provided in Table A1 in the supplementary materials. The small SD indicates that β_i is stable across folds, implying that β_i learns a consistent estimate rather than meaningless random value.

5. Usability

Our proposed SGPC is demonstrated to reduce estimation error significantly by calibrating on a few images while the user is gazing at a single point. In practice, a calibration procedure can be instructing the subject to look at one target, e.g., the camera, while moving his/her head.

For PCCR-based eye trackers, the most commonly used calibration method uses multiple calibration points [13]. This method instructs the user to gaze at different targets sequentially (typical five or nine targets). Compared to it, our proposed SGPC has two major advantages: first, SGPC is simpler and more time efficient as it only needs the user to gaze at one target. Second, it is more widely applicable.

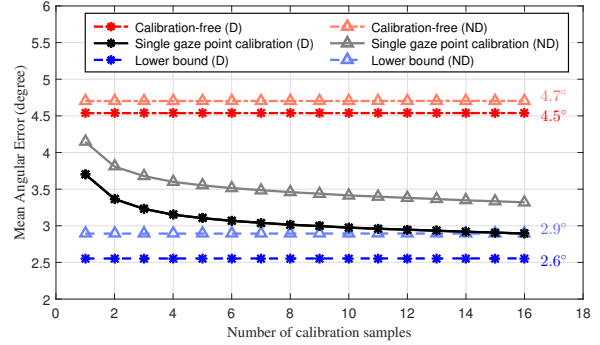


Figure 9. Comparison of the networks with/without gaze decomposition (D and ND) on the MPIIGaze dataset.

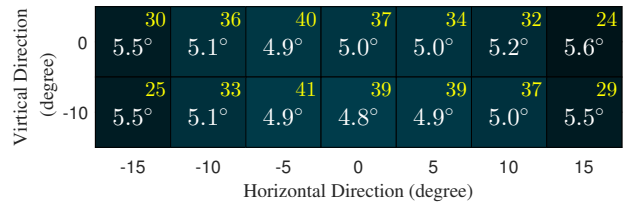


Figure 10. Mean angular error achieved by the network without gaze decomposition when calibrated at different gaze targets. Trained on the MPIIGaze and test on the Columbia dataset. $\bar{E} = 5.5^\circ$, $\underline{E} = 4.5^\circ$, $|\mathcal{D}_c| = 5$.

In some situations, e.g. screen-free applications, it is difficult to provide multiple targets for MGPC. However, with SGPC, the camera is always a visible calibration point. Although there exists a performance gap between SGPC and MGPC, we believe that SGPC provides a practically useful way to improve accuracy.

6. Conclusions

We proposed a novel gaze decomposition method for appearance-based gaze estimation. This method estimates the person-dependent bias and the gaze difference separately, which is suitable for single gaze point calibration. We conducted experiments on the MPIIGaze, the EYEDIAP and the Columbia datasets. Our results indicated that as a subject-independent estimator, the proposed method outperformed the state-of-the-art single model methods on the MPIIGaze and EYEDIAP datasets. The proposed single gaze point calibration reduced the error significantly while only requiring a few samples (about 9) looking at one point for calibration. It was also demonstrated to be quite robust to location of calibration points, where the best performance is achieved when calibrated at the center of the gaze range. Our results also demonstrate that an accurate modeling of the data can yield a significant improvement.

We believe that appearance-based gaze estimation can play an important role in many real-world scenarios, e.g.,

human-robot interaction, driver monitoring. The proposed single gaze point calibration can further reduce estimation error in a simple and time-efficient way. Potentially, the calibration may be conducted during natural interaction without giving explicit instructions to the user. Moving forward, we plan to use the results of gaze tracking to estimate the user intent. This estimated intent will enable the systems to react more naturally and to enhance the interaction.

References

- [1] D. A. Atchison, G. Smith, and G. Smith. Optics of the human eye. 2000. [2](#), [3](#)
- [2] E. Brau, J. Guan, T. Jeffries, and K. Barnard. Multiple-gaze geometry: Inferring novel 3d locations from gazes observed in monocular video. In *Proceedings of the European Conference on Computer Vision*, pages 612–630. Springer, 2018. [1](#)
- [3] Z. Chen and B. E. Shi. Appearance-based gaze estimation using dilated-convolutions. In *Asian Conference on Computer Vision*. Springer, 2018. [1](#), [2](#), [3](#), [4](#), [5](#)
- [4] Z. Chen and B. E. Shi. Using variable dwell time to accelerate gaze-based web browsing with two-step selection. *International Journal of Human-Computer Interaction*, pages 1–16, 2018. [1](#)
- [5] Y. Cheng, F. Lu, and X. Zhang. Appearance-based gaze estimation via evaluation-guided asymmetric regression. In *Proceedings of the European Conference on Computer Vision*, pages 100–115. Springer, 2018. [1](#), [2](#)
- [6] E. Chong, N. Ruiz, Y. Wang, Y. Zhang, A. Rozga, and J. M. Rehg. Connecting gaze, scene, and attention: Generalized attention estimation via joint modeling of gaze and scene saliency. In *Proceedings of the European Conference on Computer Vision*, pages 383–398. Springer, 2018. [1](#)
- [7] H. Deng and W. Zhu. Monocular free-head 3d gaze tracking with deep learning and geometry constraints. In *Proceedings of the IEEE International Conference on Computer Vision*, pages 3162–3171. IEEE, 2017. [1](#), [2](#)
- [8] J. Deng, W. Dong, R. Socher, L.-J. Li, K. Li, and L. Fei-Fei. Imagenet: A large-scale hierarchical image database. In *Proceedings of the IEEE Conference on Computer Vision and Pattern Recognition*, pages 248–255. IEEE, 2009. [4](#)
- [9] T. Fischer, H. J. Chang, and Y. Demiris. Rt-gene: Real-time eye gaze estimation in natural environments. In *European Conference on Computer Vision*, pages 334–352. Springer, 2018. [1](#), [5](#)
- [10] W. Fuhl, D. Geisler, T. Santini, T. Appel, W. Rosenstiel, and E. Kasneci. Cbf: circular binary features for robust and real-time pupil center detection. In *Proceedings of the ACM Symposium on Eye Tracking Research & Applications*, page 8. ACM, 2018. [1](#)
- [11] K. A. Funes Mora, F. Monay, and J.-M. Odobez. Eyediap: A database for the development and evaluation of gaze estimation algorithms from rgb and rgb-d cameras. In *Proceedings of the Symposium on Eye Tracking Research and Applications*, pages 255–258. ACM, 2014. [1](#), [2](#), [5](#)
- [12] A. Grillini, D. Ombelet, R. S. Soans, and F. W. Cornelissen. Towards using the spatio-temporal properties of eye movements to classify visual field defects. In *Proceedings of the ACM Symposium on Eye Tracking Research & Applications*, page 38. ACM, 2018. [1](#)
- [13] E. D. Guestrin and M. Eizenman. General theory of remote gaze estimation using the pupil center and corneal reflections. *IEEE Transactions on Biomedical Engineering*, 53(6):1124–1133, 2006. [1](#), [2](#), [3](#), [8](#)
- [14] S. Hoppe, T. Loetscher, S. A. Morey, and A. Bulling. Eye movements during everyday behavior predict personality traits. *Frontiers in Human Neuroscience*, 12:105, 2018. [1](#)
- [15] C.-M. Huang and B. Mutlu. Anticipatory robot control for efficient human-robot collaboration. In *ACM/IEEE International Conference on Human Robot Interaction*, pages 83–90. IEEE, 2016. [1](#)
- [16] S. Ioffe. Batch renormalization: Towards reducing minibatch dependence in batch-normalized models. In *Advances in Neural Information Processing Systems*, pages 1942–1950, 2017. [4](#)
- [17] D. E. King. Dlib-ml: A machine learning toolkit. *Journal of Machine Learning Research*, 10(Jul):1755–1758, 2009. [5](#)
- [18] K. Krafka, A. Khosla, P. Kellnhofer, H. Kannan, S. Bhandarkar, W. Matusik, and A. Torralba. Eye tracking for everyone. In *Proceedings of the IEEE Conference on Computer Vision and Pattern Recognition*, pages 2176–2184, 2016. [1](#), [2](#), [4](#), [5](#)
- [19] D. Lian, L. Hu, W. Luo, Y. Xu, L. Duan, J. Yu, and S. Gao. Multitask multitask gaze estimation with deep convolutional neural networks. *IEEE Transactions on Neural Networks and Learning Systems*, pages 1–14, 2018. [1](#), [2](#)
- [20] E. Lindén, J. Sjöstrand, and A. Proutiere. Appearance-based 3d gaze estimation with personal calibration. *arXiv preprint arXiv:1807.00664*, 2018. [1](#), [3](#), [6](#), [7](#)
- [21] G. Liu, Y. Yu, K. A. Funes-Mora, J.-M. Odobez, and E. T. SA. A differential approach for gaze estimation with calibration. In *British Machine Vision Conference*, 2018. [1](#), [3](#), [6](#), [7](#)
- [22] R. Menges, C. Kumar, D. Müller, and K. Sengupta. Gazetheweb: A gaze-controlled web browser. In *Proceedings of the Web for All Conference on The Future of Accessible Work*, page 25. ACM, 2017. [1](#)
- [23] B. I. Outram, Y. S. Pai, T. Person, K. Minamizawa, and K. Kunze. Anyorbit: Orbital navigation in virtual environments with eye-tracking. In *Proceedings of the ACM Symposium on Eye Tracking Research & Applications*, page 45. ACM, 2018. [1](#)
- [24] S. Park, A. Spurr, and O. Hilliges. Deep pictorial gaze estimation. In *Proceedings of the European Conference on Computer Vision*, pages 721–738. Springer, 2018. [2](#)
- [25] S. Park, X. Zhang, A. Bulling, and O. Hilliges. Learning to find eye region landmarks for remote gaze estimation in unconstrained settings. In *Proceedings of the ACM Symposium on Eye Tracking Research & Applications*, page 21. ACM, 2018. [1](#)
- [26] A. Patney, M. Salvi, J. Kim, A. Kaplanyan, C. Wyman, N. Benty, D. Luebke, and A. Lefohn. Towards foveated ren-

- dering for gaze-tracked virtual reality. *ACM Transactions on Graphics*, 35(6):179, 2016. [1](#)
- [27] J. Pi and B. E. Shi. Probabilistic adjustment of dwell time for eye typing. In *International Conference on Human System Interactions*, pages 251–257. IEEE, 2017. [1](#)
- [28] R. Ranjan, S. De Mello, and J. Kautz. Light-weight head pose invariant gaze tracking. In *IEEE Conference on Computer Vision and Pattern Recognition Workshops*, pages 2156–2164. IEEE, 2018. [1](#), [2](#)
- [29] T. Schneider, B. Schauerte, and R. Stiefelhagen. Manifold alignment for person independent appearance-based gaze estimation. In *International Conference on Pattern Recognition*, pages 1167–1172. IEEE, 2014. [2](#)
- [30] A. Shrivastava, T. Pfister, O. Tuzel, J. Susskind, W. Wang, and R. Webb. Learning from simulated and unsupervised images through adversarial training. In *Proceedings of the IEEE International Conference on Computer Vision*, pages 2242–2251. IEEE, 2017. [1](#)
- [31] K. Simonyan and A. Zisserman. Very deep convolutional networks for large-scale image recognition. *arXiv preprint arXiv:1409.1556*, 2014. [4](#)
- [32] B. A. Smith, Q. Yin, S. K. Feiner, and S. K. Nayar. Gaze locking: passive eye contact detection for human-object interaction. In *Proceedings of the ACM Symposium on User Interface Software and Technology*, pages 271–280. ACM, 2013. [1](#), [2](#), [7](#)
- [33] Y. Sugano, Y. Matsushita, and Y. Sato. Learning-by-synthesis for appearance-based 3D gaze estimation. In *Proceedings of the IEEE Conference on Computer Vision and Pattern Recognition*, pages 1821–1828. IEEE, 2014. [1](#), [2](#)
- [34] H. Wang, J. Pi, T. Qin, S. Shen, and B. E. Shi. SLAM-based localization of 3D gaze using a mobile eye tracker. In *Proceedings of the ACM Symposium on Eye Tracking Research & Applications*, page 65. ACM, 2018. [1](#)
- [35] K. Wang and Q. Ji. Real time eye gaze tracking with 3d deformable eye-face model. In *Proceedings of the IEEE International Conference on Computer Vision*, pages 1003–1011, 2017. [1](#)
- [36] K. Wang, R. Zhao, and Q. Ji. A hierarchical generative model for eye image synthesis and eye gaze estimation. In *The IEEE Conference on Computer Vision and Pattern Recognition*, June 2018. [1](#)
- [37] E. Wood, T. Baltrušaitis, L.-P. Morency, P. Robinson, and A. Bulling. Learning an appearance-based gaze estimator from one million synthesised images. In *Proceedings of the ACM Symposium on Eye Tracking Research & Applications*, pages 131–138. ACM, 2016. [1](#)
- [38] F. Yu and V. Koltun. Multi-scale context aggregation by dilated convolutions. *arXiv preprint arXiv:1511.07122*, 2015. [4](#)
- [39] Y. Yu, G. Liu, and J.-M. Odobez. Deep multitask gaze estimation with a constrained landmark-gaze model. In *European Conference on Computer Vision*, pages 456–474. Springer, 2018. [2](#)
- [40] X. Zhang, Y. Sugano, and A. Bulling. Revisiting data normalization for appearance-based gaze estimation. In *Proceedings of the ACM Symposium on Eye Tracking Research & Applications*, page 12. ACM, 2018. [5](#)
- [41] X. Zhang, Y. Sugano, M. Fritz, and A. Bulling. Appearance-based gaze estimation in the wild. In *Proceedings of the IEEE Conference on Computer Vision and Pattern Recognition*, pages 4511–4520, 2015. [1](#), [2](#), [3](#), [5](#), [11](#)
- [42] X. Zhang, Y. Sugano, M. Fritz, and A. Bulling. Its written all over your face: Full-face appearance-based gaze estimation. In *IEEE Conference on Computer Vision and Pattern Recognition Workshops*, pages 2299–2308. IEEE, 2017. [1](#), [2](#), [5](#)
- [43] X. Zhang, Y. Sugano, M. Fritz, and A. Bulling. MPIIGaze: Real-world dataset and deep appearance-based gaze estimation. *IEEE Transactions on Pattern Analysis and Machine Intelligence*, 41(1):162–175, 2019. [1](#), [2](#), [6](#), [7](#)

		P1		P2		P3		P4		P5		P6		P7		P8	
Yaw	Mean($^{\circ}$)	2.8	-2.8	1.2	-1.2	0.3	-0.4	0.2	-0.2	-1.8	1.9	-4.1	4.0	-0.7	0.7	1.4	-1.5
	SD($^{\circ}$)	0.2	0.3	0.3	0.1	0.1	0.2	0.1	0.1	0.1	0.1	0.2	0.1	0.1	0.1	0.1	0.2
Pitch	Mean($^{\circ}$)	0.0	0.0	-0.8	-0.8	3.9	3.9	-1.7	-1.8	0.1	0.1	-0.5	-0.4	-1.5	-1.6	0.3	0.3
	SD($^{\circ}$)	0.2	0.2	0.3	0.3	0.3	0.3	0.2	0.2	0.2	0.2	0.2	0.2	0.2	0.2	0.2	0.2
		P9		P10		P11		P12		P13		P14		P15			
Yaw	Mean($^{\circ}$)	-3.5	3.4	-0.7	0.9	-0.3	0.2	0.9	-0.9	-0.4	0.3	1.9	-1.8	5.4	-5.4		
	SD($^{\circ}$)	0.1	0.1	0.3	0.2	0.1	0.2	0.2	0.2	0.1	0.2	0.1	0.1	0.1	0.1		
Pitch	Mean($^{\circ}$)	-0.6	-0.7	1.7	1.8	-2.9	-2.9	1.8	1.7	0.2	0.2	-2.8	-2.8	2.9	2.9		
	SD($^{\circ}$)	0.2	0.2	0.3	0.3	0.2	0.3	0.3	0.3	0.1	0.2	0.2	0.2	0.2	0.2		

* For each subject, the left column corresponds to the non-flipped images and the right column corresponds to the horizontally-flipped images.

Table A1. Mean and standard deviation (SD) of the learned bias β for each subject across 14 folds on the MPIIGaze dataset [41].

A. Appendix

We evaluated whether the learned biases, i.e., β_i in (4) were consistent for the same subject using leave-one-subject-out (15 fold) cross-validation on the MPIIGaze dataset. For each subject, we computed the mean and SD of the bias across the 14 folds where the subject was included in the training set. The mean and SD of each subject are shown in Table A1. Across subjects, the yaw means ranged from -5.4° to 5.4° (SDs from 0.1° to 0.3°). The pitch means ranged from -2.9° to 3.9° (SDs from 0.1° to 0.3°). The small SD indicates that β_i is stable across folds, implying that β_i learns a consistent estimate rather than meaningless random value.